Renewable Energy 204 (2023) 774–787

Contents lists available at ScienceDirect

Renewable Energy

journal homepage: www.elsevier.com/locate/renene

Prediction of thermal degradation of biopolymers in biomass under pyrolysis atmosphere by means of machine learning

Furkan Kartal, Yağmur Dalbudak, Uğur Özveren *

Department of Chemical Engineering, Marmara University, Goztepe Campus, 34722, Kadikoy, Istanbul, Turkey

ARTICLE INFO

Keywords:
Biopolymers
Biomass
Thermal degradation
Artificial neural networks
Biomass characterization

ABSTRACT

Biomass is the most widespread among renewable energy sources and offers many advantages. However, the heterogeneous structure of biomass brings many disadvantages. Therefore, characterization of thermal degradation of biopolymeric structures in biomass such as hemicellulose (HC), cellulose (CL), and lignin (LN) is very important for the efficiency of any biomass-based thermal process. On the other hand, the characterization of these biopolymers requires various experimental procedures that consume resources and time. Artificial neural networks (ANN) as a machine learning approach provide a remarkable opportunity to identify patterns in the complex structure of biomass fuels and their thermochemical degradation processes. In this study, a new model was developed for the first time to generate differential thermogravimetric analysis (DTG) curves for HC, CL and LN in biomass using proximate analysis results of raw biomass. DTG curves were evaluated using a ANN model developed with the open-source "TensorFlow" library in Python software. ANN model performed excellently with R^2 values above 0.998. The results show that the newly developed model can estimate the thermal degradation for any temperature, so that biopolymer fractions in the degraded biomass can be calculated immediately, which has not been reported before.

1. Introduction

Despite the fact that fossil fuels are still widely used today [1], the unrestricted use of fossil fuels has serious consequences such as environmental pollution, toxic gas emissions and accelerated climate change due to increased greenhouse gas concentrations, etc. [2]. Due to its physicochemical properties, biomass is the only substitute for coal among renewable energy sources. Therefore, researchers are encouraged to pursue biomass conversion technologies through research and development. However, to achieve effective utilization of biomass, it is absolutely critical to properly characterize the biomass, i.e., determine its composition.

The use of biomass contributes less to greenhouse gas concentrations than fossil fuels, and it is carbon neutral, biodegradable, and abundant [3]. On the other hand, the presence of various forms in nature brings diverse disadvantages to biomass. Examples of these disadvantages include high moisture content, calorific value in a wide scale, need for large volume for storage, and relatively low energy density [4]. Therefore, large-scale applications of biomass are limited. Nonetheless, biomass is traditionally defined as a chemical combination of three biopolymeric components: lignin (LN), cellulose (CL), and hemicellulose (HC) [5].

CL microfibrils are one of the most important compounds discovered in plant cell walls. CL is divided into three main categories based on its solubility and degree of polymerization; α- CL, β- CL and γ- CL [6]. Similar to CL, HC is another major component that makes up plant cell walls, but HC is more complex than CL [7]. HC is comprised of a set of heterogeneous polysaccharides that have more branching and a lower degree of polymerization than CL. In lignocellulosic biomass, LN is a phenolic polymer. When an enzyme must interact on a lignocellulosic carbohydrate component, it produces a physical barrier [8]. LN also provides structural strength to a plant and defends it from microbial attack. Although it varies, the ratio of biopolymers in many plants is 23–32% for HC, 38–50% for CL, and 10–25% for LN [9]. These three key chemical components of biomass have an effect on the thermochemical system's performance, which in turn affects the efficiency of the biomass-based power system [10]. As a result, the proportions of these three main chemical constituents must be defined.

Depending on the operating parameters of the thermal degradation process, several significant product and yield variations are possible [11]. The complexity of the final product is enhanced by the

* Corresponding author.
E-mail address: ugur.ozveren@marmara.edu.tr (U. Özveren).

https://doi.org/10.1016/j.renene.2023.01.017
Received 3 March 2022; Received in revised form 2 January 2023; Accepted 5 January 2023
Available online 10 January 2023

Abbreviations

HC	Hemicellulose
CL	Cellulose
LN	Lignin
ANN	Artificial neural network
DTG	Derivative thermogravimetric curve
NIR	Near-infrared spectroscopy
VIS	Visible spectroscopy
TGA	Thermogravimetric analysis
ASTM	American Society for Testing and Materials
a.r.	As received basis
d.b.	Dry basis
wt	Weight
MLP	Multilayer perceptron
ReLU	Rectified linear unit
SELU	Scaled exponential linear unit
MSE	Mean squared error
MAPE	Mean absolute percentage error
VM	Volatile matter
FC	Fixed carbon
M	Moisture

heterogeneity of the biomass, which is mainly composed of three polymers. In other words, both the properties of the thermally treated solid material and the yield of the products to be obtained at the end of the thermochemical process are highly influenced by the operating conditions and the content of the raw biomass sample [12]. At low temperatures (<553 K), hemicellulose decomposes by dehydration, for example, while at higher temperatures, it decomposes by depolymerization [13]. In lignin degradation, dehydration is the most important step at low temperatures, but at higher temperatures, a variety of lignin monomers are formed. At temperatures above 773 K, the monomers decompose and enter the gaseous state. Compared to cellulose and hemicellulose, lignin is more thermally stable, produces more char, and has a higher aromatic chemical yield [14]. Moreover, at low temperatures (<623 K) and modest heating rates, dehydration is the primary mechanism in the cellulose degradation process. The processes of depolymerization and fragmentation take precedence at elevated temperatures. At temperatures between 573 and 723 K, depolymerization predominates, whereas at roughly 873 K, fragmentation is at its most efficient [12]. These results show that the operating temperature has a significant effect on the degradability of biomass, especially on the biopolymers it contains. Therefore, it is critical to determine the proper thermal degradation temperature to predict the biopolymer content of products to be evaluated for further applications. In addition to the operating conditions, proximate analysis results also provide information on the HC, LN and CL content of the biomass.

In these three biopolymers, numerous chemical bonds are broken during thermolysis, releasing their volatile components [15]. A number of studies have demonstrated that volatiles are primarily produced during the depolymerization process [16–18]. A particularly important aspect of thermolysis is the formation of aromatic rings (especially benzene rings), since they significantly contribute to char formation [19,20]. Shen et al. [21] found that slow heating rates result in higher char yields from the pyrolysis of cellulose. In summary, the studies based on thermal analysis have shown the effects of biopolymers in lignocellulosic fuels on biomass volatiles and char (fixed carbon and ash).

Several experimental approaches for determining the weight percentage of HC, CL, and LN have been published in the literature [22–26]. A conventional wet chemical analysis is carried out using a variety of acidic reagents and alkaline such as H_2SO_4, KOH, and others to evaluate the anticipated content's weight in relation to the three main components [27]. While wet chemical analysis is an effective method for estimating the weight of complex compounds, it is an empirical procedure, variations in technique affect the final result [28]. Near-infrared reflectance (NIR) spectroscopy is frequently used for determining nutritional content and analyzing the composition of plant materials, medicines, foods, and animals [29]. The visible (VIS) and NIR spectroscopy wavelengths have also been employed to determine main biopolymers in biomass cell walls. NIR spectroscopy is well-known as a quick and easy way to do analysis [30], although the most common method for identifying chemical constituents is to construct partial least squares regression models between absorbance and measured biomass chemical compounds at specific wavelengths [31]. Another approach for determining three macromolecules in biomass is thermogravimetric analysis (TGA). The TGA technique can determine thermal decomposition zones for each component and quantitatively resolve complex mixtures [32].

All of these experimental techniques, however, are costly, time-consuming, and not financially viable, and testing apparatus may not be accessible to everyone [33]. Therefore, generalized correlations have been established to minimize the time and resource consumption. In addition, researchers have recently developed various computational methods, especially in the context of machine learning. Using the elemental H:C and O:C ratios, as well as the proportion of volatiles in the proximate analysis result, Sheng et al. [5] used nonlinear correlations for estimating the LN and CL mass percentages. The authors indicated that the correlation coefficient was 90% for CL and 81% for LN. To forecast HC, CL, and LN, Xing et al. [31] created a new random forest model. The researchers used 144 samples from the literature as input variables, including elemental carbon, hydrogen, oxygen percentages, and the H:C and O:C ratios. The coefficients of determination of the random forest model were calculated as 0.954 for CL, 0.933 for HC and 0.968 for LN. Carrier et al. [34] developed correlations by performing thermogravimetric analysis to determine the amount of macromolecules in a biomass sample. The correlations were successful in determining α-CL and HC, but failed because they reported large deviations in determining LN. In a recent study, Nimmanterdwong et al. [6] developed a mathematical model that predicts HC, CL and LN content using the ultimate/proximate information of biomass with the dataset they created by reviewing the literature. They also applied the self-organizing map technique (data clustering) to improve the performance of the regression model they developed. According to the authors, the model they developed is effective in reducing the resources and time spent.

Despite the fact that biomass samples are usually identified as the chemical combination of LN, HC, and CL, the quantitative distribution of these three biopolymeric components in solid material is important for further applications. Therefore, many researchers have used computational approaches to both determine the ratios of these three biopolymers in solid materials and to reduce the time and cost of experiments. Although estimates of the amount of the three major biopolymers in biomass have already been made using various input variables, no study has yet been presented on the estimation of the proportion in biomass by simulating the thermal degradation of HC, CL, and LN in biomass using the results of the proximate analysis of the raw biomass. In other words, while the models described in the literature cover only the prediction of the biopolymer content of the raw biomass, they do not include an estimation of the CL, LN and HC content of a solid material that is degraded and changes its structure/content under the influence of temperature. The ANN model proposed in this study makes predictions of the biopolymer content for the biomass sample decomposed at a given temperature using the proximate analysis results, which can be obtained relatively easily from the ultimate analysis, as the input variable. In this study, thermogravimetric characterization of eight different biomass samples was performed and a dataset with temperature vs. mass change/time points was generated. In this way, the thermal degradation process of HC, CL and LN can be simulated considering the biomass characteristics in a certain temperature/temperature range

Table 1
The ultimate and proximate analysis results of the biomass samples.

Feedstock Material	Proximate Analysis (a.r., wt.%[a])				Ultimate Analysis (d.b., wt.%[b])				
	M	FC	VM	Ash	C	H	N	S	O
Hazelnut Shell	3.07	25.32	70.76	0.85	41.65	5.58	0.50	2.34	49.05
Hazelnut Husk	3.96	22.89	64.45	8.70	41.39	5.27	0.86	2.15	41.27
Almond Shell	2.27	20.02	76.51	1.20	45.16	5.72	0.15	3.04	44.70
Barley Straw	2.68	14.14	69.67	13.51	36.40	5.12	0.49	3.07	41.03
Wheat Straw	2.35	15.52	67.71	14.42	36.83	5.12	0.74	2.19	40.34
Olive Pomace	3.08	21.51	68.60	6.81	47.40	5.73	1.54	2.14	36.17
Rice Husk	3.92	13.86	63.10	19.12	37.49	5.15	0.89	1.54	35.03
Rice Straw	2.73	14.77	68.70	13.80	39.44	5.27	0.81	2.11	38.18

[a] a.r., wt.%: as received, weight %.
[b] d.b., wt.%: dry basis, weight %.

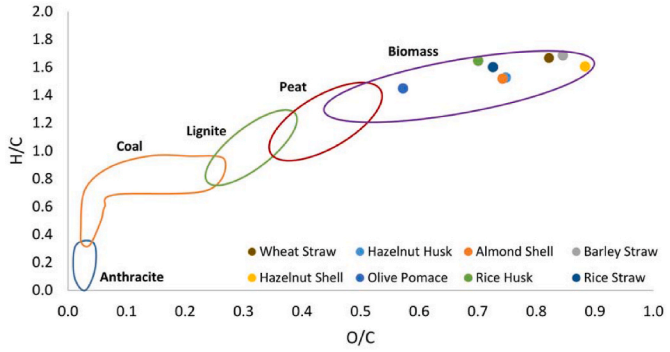

Fig. 1. Characterization of biomass samples by Van Krevelen diagram.

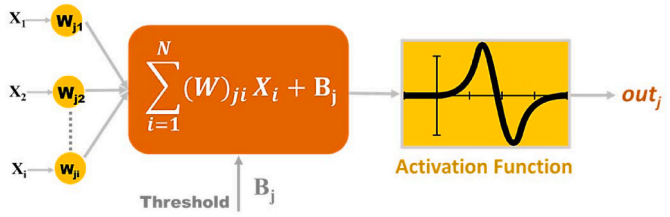

Fig. 2. Architecture of an artificial neuron.

without an experimental procedure. In addition, estimation of biopolymer thermal degradation curves in biomass as a function of temperature will allow researchers to develop more advanced biomass energy recovery processes.

2. Materials and methods

2.1. Feedstock characterization

Local farmers in the Turkish Aegean region provided the biomass samples used for this study. In order to perform fuel characterization, proximate analysis and ultimate analysis experiments were conducted in American Society for Testing and Materials (ASTM) standards. Proximate analysis (moisture (M), fixed carbon (FC), volatile matter (VM), and ash) was performed using NETZSCH STA 409 PC Luxx thermogravimetric analyzer, while ultimate analysis (carbon (C), hydrogen (H), nitrogen (N), and sulphur (S)) was performed using LECO Truspec microelemental analyzer at Advanced Technologies Application and Research Center, Hacettepe University. The oxygen content, on the other hand, was calculated using Eq. (1):

$$O\ (\%) = 100 - (Ash + N + H + S + C) \quad (1)$$

With respect to which the dry base values for ash, C, H, S, and N are

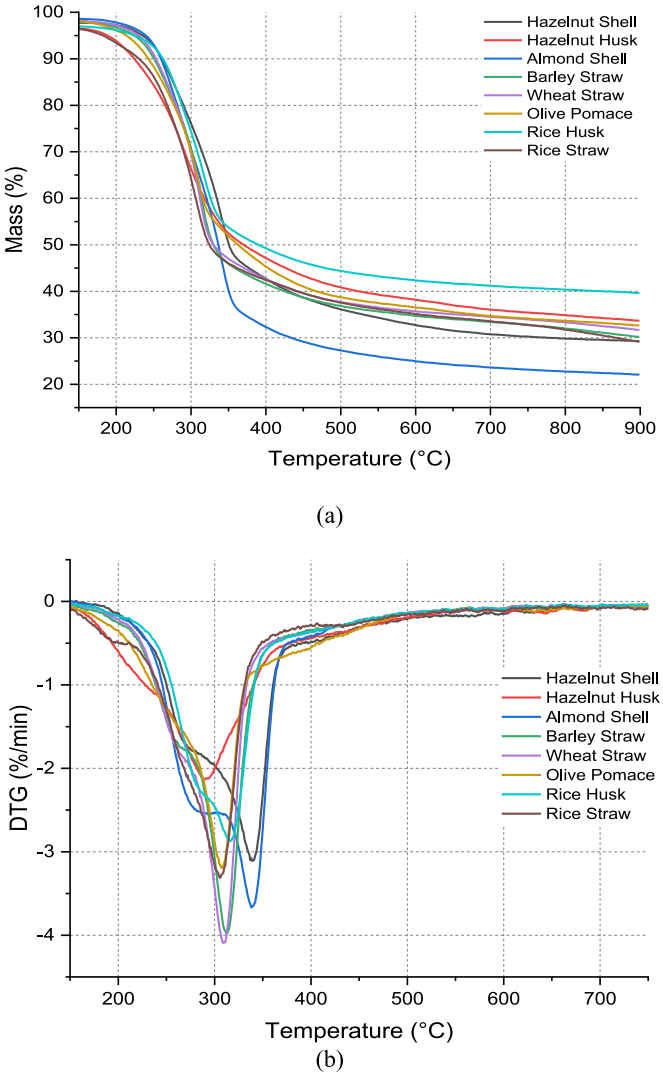

Fig. 3. TG (a) and DTG (b) profiles of biomass samples.

provided. Table 1 summarizes the feedstock material's ultimate and proximate analysis results.

High VM content as a general characteristic of biomass is also a common feature of all biomass samples listed in Table 1 (above 60%). This is an indicator that biomass is a suitable fuel for the pyrolysis process. In addition, the low N content makes the fuel valuable as it potentially produces lower amounts of NO_x. Among the biomass samples, straw forms have higher ash content, which is an expected outcome [35]. On the other hand, rice husk stands out as the material with the

Table 2
Thermogravimetric characteristics of feedstock materials for the pyrolysis process.

Feedstock Material	Mass Loss in the First Step (%)	Mass Loss in the Second Step (%)	Residual Mass (%)	First Peak/ Hemicellulose Shoulder (%/min, °C)	Second Peak/ DTG_{max} (%/min, °C)
Hazelnut Shell	51.76	15.57	29.32	1.76, 273.7	3.11, 339.1
Hazelnut Husk	46.10	14.91	33.69	1.11, 238.0	2.14, 289.5
Almond Shell	63.35	11.88	22.11	2.56, 294.6	3.67, 337.8
Barley Straw	51.83	12.84	30.24	1.75, 264.4	3.98, 311.8
Wheat Straw	49.79	13.41	31.70	1.85, 265.7	4.11, 310.5
Olive Pomace	43.67	19.82	32.70	1.53, 263.8	3.20, 307.4
Rice Husk	42.97	12.64	39.67	2.29, 287.0	2.87, 316.8
Rice Straw	49.26	13.76	29.15	1.99, 267.5	3.32, 305.8

highest ash content among all biomass samples, with an ash content of 19.12%. Fig. 1 shows the Van Krevelen diagram for the biomass samples used in this work.

The Van Krevelen diagram is a technique employed to identify solid fuels, particularly for determining their carbonization degree [36]. By calculating the O:C and H:C values of solid fuels, their membership in a particular class can be seen in the diagram, and information about their quality can be obtained. Olive pomace had low H:C and O:C values, which puts it close to the peat field as a relatively high-quality fuel.

2.2. Experimental apparatus

The TGA tests were conducted using the characterized feedstock materials. Before the TGA operation, the biomass sample was dried for 24 h at 105 °C, pulverized, and sieved below 250 μm. The grinding process was carried out with the "IKA M20 Universal Mill". In the instrument's heating chamber, an aluminum oxide crucible with a sample of approximately 10.000 ± 1.000 mg was attached and monitored for stabilization. Afterwards, the non-isothermal heating procedure with a heating rate of 5 °C/min from 25 °C to 900 °C were carried out with the thermogravimetric analyzer "NETZSCH STA 409 PC Luxx". The pyrolysis tests were carried out in a purified argon atmosphere, with the carrier gas flow rate set at 45 mL/min throughout the thermolysis operations (15 mL/min for the balance and 30 mL/min for the heating chamber). During the pyrolysis processes, the quantitative evaluation of the samples was recorded using the software "STA 409 PC" based on the TGA and derivative thermogravimetric (DTG) curves.

2.3. Artificial neural networks

ANNs are the networks that relate the inputs and outputs of a system, and these networks have been successfully used to map nonlinear input and output relationships in a variety of applications [37]. ANNs are computational systems inspired by the brain and nervous system that offer certain advantages over regression-based models, including the ability to process noisy data. ANNs have recently gained popularity in solving difficult, real-world engineering and scientific problems due to their strong generalization capabilities [38]. The ANN method, which has its origins in mathematical neurobiology, and its hybrids can be

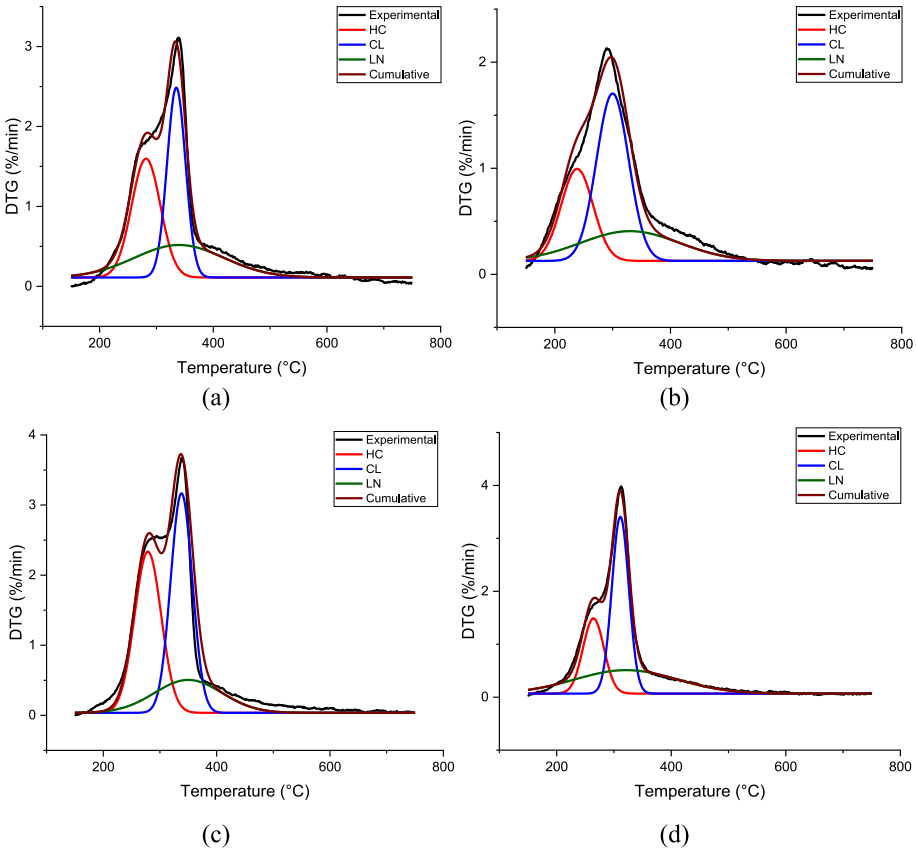

Fig. 4. Visualization of the distributions of biomass pseudo components.
(a) Hazelnut Shell, (b) Hazelnut Husk, (c) Almond Shell, (d) Barley Straw, (e) Wheat Straw, (f) Olive Pomace, (g) Rice Husk, (h) Rice Straw..

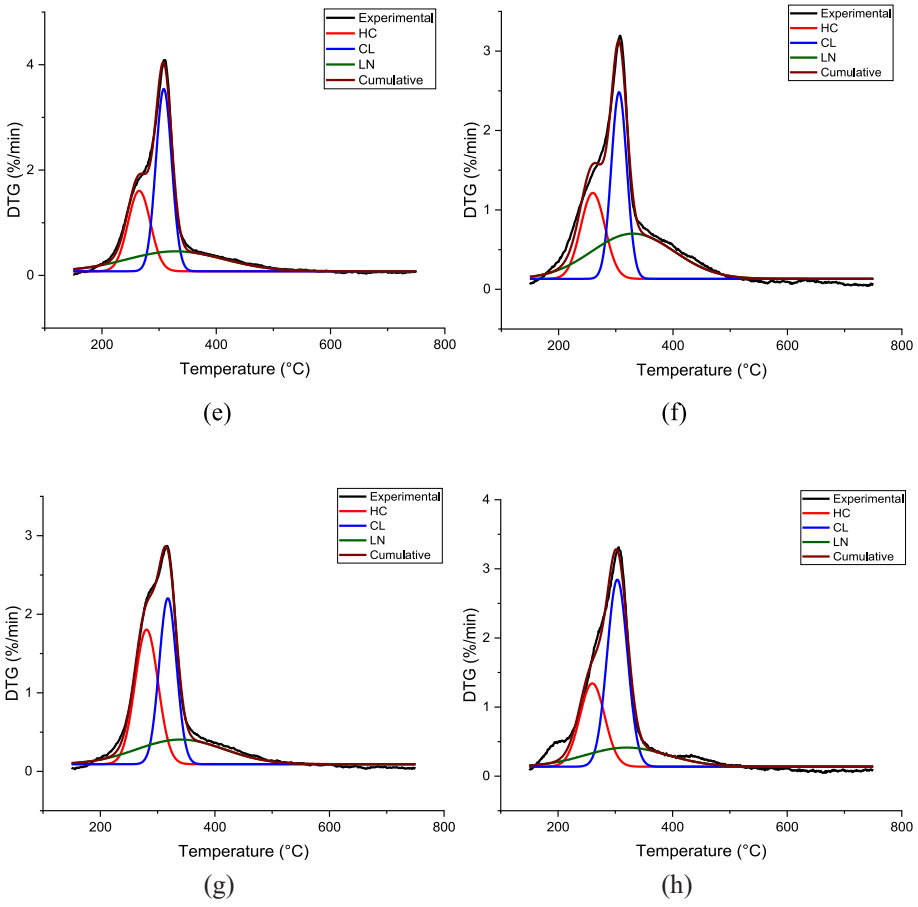

Fig. 4. (*continued*).

promising candidates for dealing with nonlinear systems and complex systems problems, especially when faced with unclear, noisy, incomplete, or unknown data patterns [39]. Without having to learn the underlying mechanics and principles, ANN-based modeling systems may be able to quickly and accurately map complex processes from a number of cases. To put it another way, ANN-based models can explain intricate dynamic systems with multidimensional properties without having a detailed knowledge of the underlying physical principles [40]. The approaches used in conventional modeling are quite different from those used in ANN. Unlike the conventional approach, ANN uses input data to collect and evaluate data [40].

Multilayer perceptrons (MLPs) with backpropagation learning algorithms are the most widely used ANN models for a variety of problems. They are essentially based on the supervised method and consist of three layers: input, hidden, and output. The nodes of each layer are fully connected to the nodes of the next layer via weights. To achieve the lowest possible model error, the training method iteratively adjusts the weights between nodes. A variety of training methods are available for efficient training, such as gradient descent algorithm, Levenberg-Marquardt algorithm, stochastic gradient descent algorithm, etc. [41]. In ANN, the basic processing element is a perceptron, which can be configured in various ways and contains the calculations and generates output values. The processing elements (also called perceptron, neuron and node) are connected to other processing elements. Fig. 2 shows a schematic representation of a perceptron.

The perceptron multiplies the input variables by a weight value and converts them to output values in the corresponding layer. The outcome of this multiplication is then given a bias value. The initial bias and weight values are generally chosen at random. Eq. (2) can be used to express a neuron's output:

$$out_j = h\left(\sum_{i=1}^{N} W_{ji}X_i + b_j\right) \tag{2}$$

where W_{ji} is the weight of the link from the i_{th} node of the previous layer to a j_{th} node of the current layer, and b_j is the bias, X_i is the previous layer's i_{th} node's output. The training procedure is used to generate the network weights W_{ji} and biases b_j. To minimize the difference between the targeted output and the actual output, a suitable activation function, indicated as h, must be selected. The activation (transfer) function reduces the amplitude of received signal to a predetermined threshold. The activation function can have either a linear or a nonlinear shape. Unity step, sigmoid, Gaussian, tangent, piecewise linear, and hyperbolic tangent are the most common transfer functions in ANNs. Rectified linear unit (ReLU) [42] and scaled exponential linear unit (SELU) [43] were chosen as activation functions in this study.

$$SELU(x) = \lambda\begin{cases} x, if\ x > 0 \\ ae^x - a, otherwise \end{cases} \tag{3}$$

where α is 1.67 and λ is 1.05

$$ReLU = \max\ (0, x) \tag{4}$$

Inputs and trainable parameters are mapped to a range from −1 to 1 by the tangent hyperbolic function, while the sigmoid activation function maps trainable parameters to a range from 0 to 1. Saturation zones are represented by these functions when inputs cause output values to approach limits. A potential problem is that the gradient is too small, known as vanishing gradients, when the input causes the output to fall off in these regions, as shown by the backpropagation process. When a network encounters vanishing gradients, it cannot learn because its

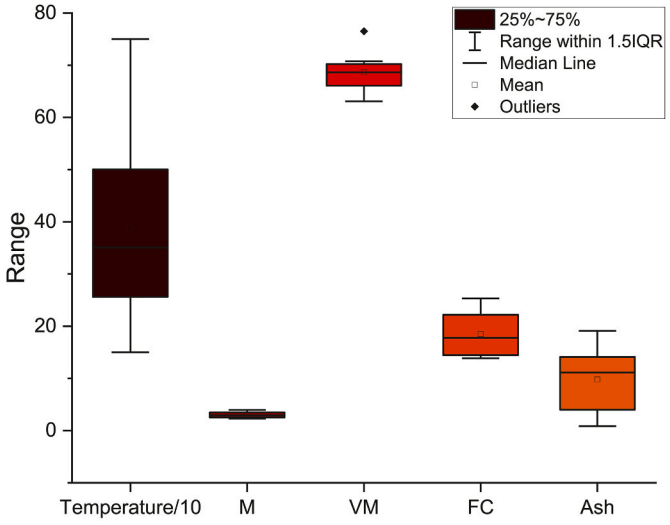

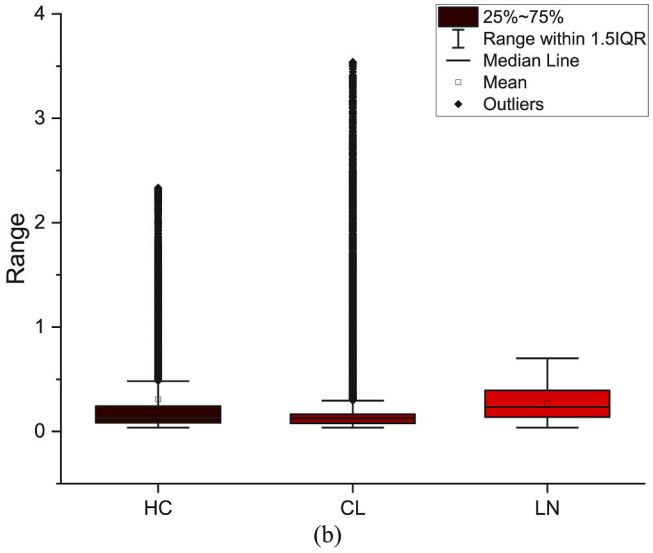

Fig. 5. Boxplots of input and output parameters. (a) Input parameters, (b) Output parameters.

Table 3
A statistical description of the dataset.

	Mean	Standard Deviation	Minimum	Maximum
Temperature (°C)	388.81	162.75	150	750
M	3.01	0.6	2.27	3.96
VM	68.69	3.82	63.1	76.51
FC	18.5	4.19	13.86	25.32
Ash	9.8	6.15	0.85	19.12
HC	0.308875	0.432539	0.03562	2.33521
CL	0.389425	0.687537	0.03562	3.53975
LN	0.267028	0.155002	0.03562	0.70127

trainable parameters are not changed. Conversely, ReLU can avoid vanishing gradients because its output is zero for values below zero and one otherwise. Moreover, ReLU helps to speed up the training process, minimize computational cost, and avoid the common phenomenon of vanishing gradients. Moreover, SELU is a useful transfer function to speed up convergence and thus training time when the inputs and outputs of all layers in a network model have a normal distribution. Based on this concept, the SELU activation function is designed to provide

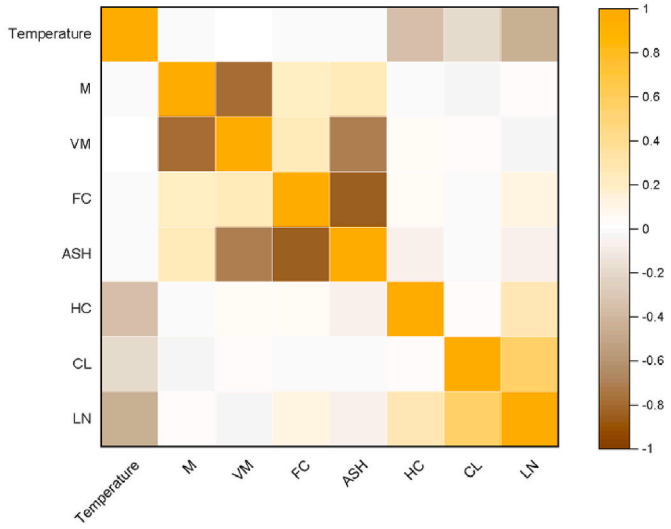

Fig. 6. A heat map for the input and output parameters.

normally distributed results. In other words, the function helps to map the mean and variance of the output at each layer of the network to be statistically close to the normal distribution.

The two main aspects of ANN training are the forward propagation of the signal and the backward propagation of the error. The global error is computed after the forward propagation of the data, and if it exceeds the target error, it is backward propagated, adjusting the biases and weights of each layer. The backward propagation of the error is determined as follows:

$$E = \frac{1}{2}\sum_{i=1}^{n}\left(y_i^d - y_i^p\right)^2 \tag{5}$$

$$w_{ij}(k+1) = w_{ij}(k) - \eta\frac{\partial E(k)}{\partial w_{ij}(k)} \tag{6}$$

$$b_{ij}(k+1) = b_{ij}(k) - \eta\frac{\partial E(k)}{\partial b_{ij}(k)} \tag{7}$$

where y_i^d is the ANN's expected output, y_i^p is the ANN's output, E is the global error, η is the learning rate, $b_{ij}(k)$ and $w_{ij}(k)$ are the k-th iteration's connection biases and weights across layers, respectively.

As an optimizer, Adamax algorithm [44] was selected in this study. Adaptive moment estimation, from which the name Adam is derived, is a method for fast stochastic optimization that uses only first-order gradients and minimal memory. From the estimated first and second moments of the gradients, the method determines individual adaptive learning rates for each parameter. Adam has several advantages, including the fact that its step sizes are approximately constrained by the step size hyperparameter, that it can work with sparse gradients, that it does not require a stationary target, and that it automatically performs some form of step size annealing. Adam's weights are updated using a gradient scaling method that is inversely proportional to the (scaled) norm of the recent and past gradients of each weight. In other words, Adamax is an infinity norm based extension of the Adam algorithm [45]:

$$Adam: \; m_n = E[A^n] \tag{8}$$

where m represents the moment of that particular variable, A represents any variable, and E represents the expected value of n variables.

$$Adamax: \; v_t = \beta_2 v_t + (1-\beta_2)|g_t|^2 \tag{9}$$

$$u_t = \beta_2^{\infty} v_{t-1} + \left(1-\beta_2^{\infty}\right)|g_t|^{\infty} \tag{10}$$

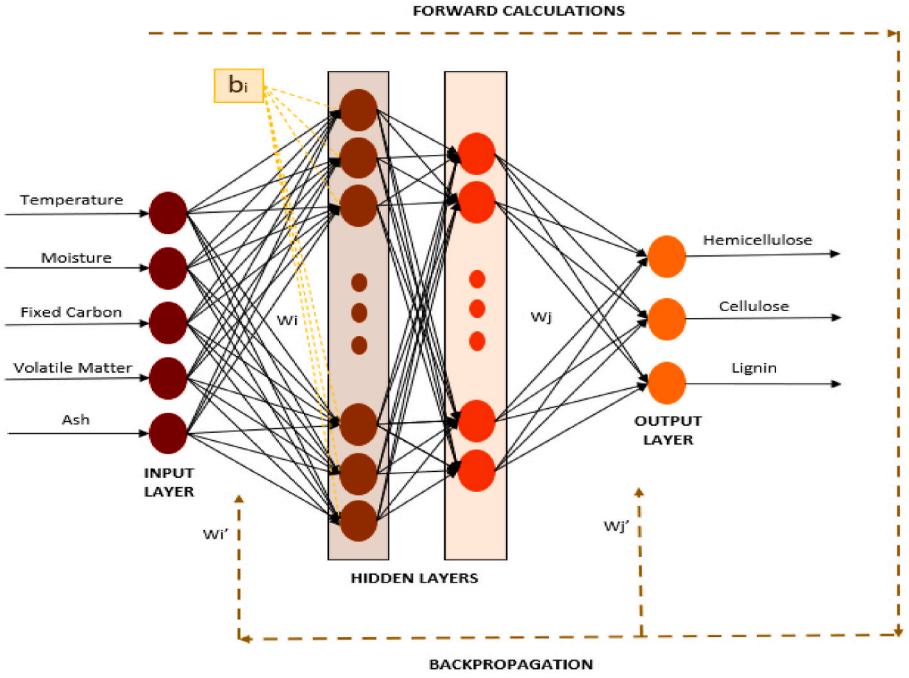

Fig. 7. The neural network topology that was employed to forecast DTG points of HC, CL, and LN.

Table 4
The parameters of the ANN model that developed in this study.

Parameter	Value
Number of neurons in the input layer	5
Number of neurons in the first hidden layer	150
Number of neurons in the second hidden layer	100
Number of neurons in the output layer	3
Type of the neural network	Feed Forward Backpropagation
Transfer function in the first hidden layer	ReLU
Transfer function in the second hidden layer	SELU
Loss function	MSE
Optimization algorithm	Adamax
Number of dataset	8000
Data division (training, test)	Random (6400, 1600)

$$u_t = \max\left(\beta_2 . v_{t-1}, |g_t|\right) \tag{11}$$

where v_t stands for updating of norms and u_t examines the extensiveness of norm v_t.

2.4. Statistical evaluation indicators

The difference between the predicted and calculated values can be used to quantify error. The bias and weight coefficients of the preceding layer are readjusted in combination with the backpropagation errors to decrease backpropagation errors. As a result, the neural network accurately predicts new instances by improving the performance. When evaluating errors, the researchers employed the coefficient of determination (R^2) in Eq. (12), the mean squared error (MSE) in Eq. (13), and the mean absolute percentage error (MAPE) in Eq. (14):

$$R^2 = 1 - \frac{\sum_{i=1}^{n}\left(Y_{predicted} - Y_{observed}\right)^2}{\sum_{i=1}^{n}\left(Y_{predicted} - Y_{mean}\right)^2} \tag{12}$$

$$MSE = \frac{1}{n}\sum_{i=1}^{n}\left(Y_{predicted} - Y_{observed}\right)^2 \tag{13}$$

$$MAPE = \frac{100}{n}\sum_{i=1}^{n}\left|\frac{Y_{observed} - Y_{predicted}}{Y_{observed}}\right| \tag{14}$$

where the number of instances, the value generated by the ANN model, the observed value, and the average value of the observed outputs are symbolized by n, $Y_{predicted}$, $Y_{observed}$, and Y_{mean}, respectively.

3. Results

3.1. TGA results

Thermal decomposition of solid fuels is very complicated, and primary and secondary pyrolysis regions are often present. During the decomposition of HC and CL, the primary pyrolysis zone mainly produces lighter volatiles and tar. In the secondary pyrolysis zone, on the other hand, the final char is formed when the more tightly bound components (mainly LN) are cracked at higher temperatures. Fig. 3 shows the TG (a) and DTG (b) plots of biomass samples at a heating rate of 5 °C/min. Although all biomass samples have a similar number of degradation steps, the TG and DTG curves have different characteristics. The TG curves (Fig. 3a) show large mass losses, especially at temperatures below 350 °C, while the DTG curves (Fig. 3b) show one or more prominent peaks depending on the structure of the biomass. In the primary pyrolysis step, HC (<350 °C) and CL (250–500 °C) are thermally degraded [46].

In general, HC is seen as a shoulder rather than a peak in the DTG curve, so the peak temperature (DTG_{max}) belongs to CL degradation [47]. Since the organic compounds of the biomass are linked by ether bonds (R-O-R), which have poor thermal resistance, significant mass losses occur at this step. In addition to the production of large amounts of non-condensable gas, hydrocarbon and tar, the primary pyrolysis zone also produces semi-coke [48]. The gradual degradation characteristics across a wider temperature range, however, meant that there was no obvious peak in the secondary pyrolysis zone. At elevated temperatures (>400 °C), the secondary pyrolysis stage represents the region where stronger components are fractured [49]. The thermogravimetric properties of the biomass samples for the pyrolysis process are summarized in Table 2.

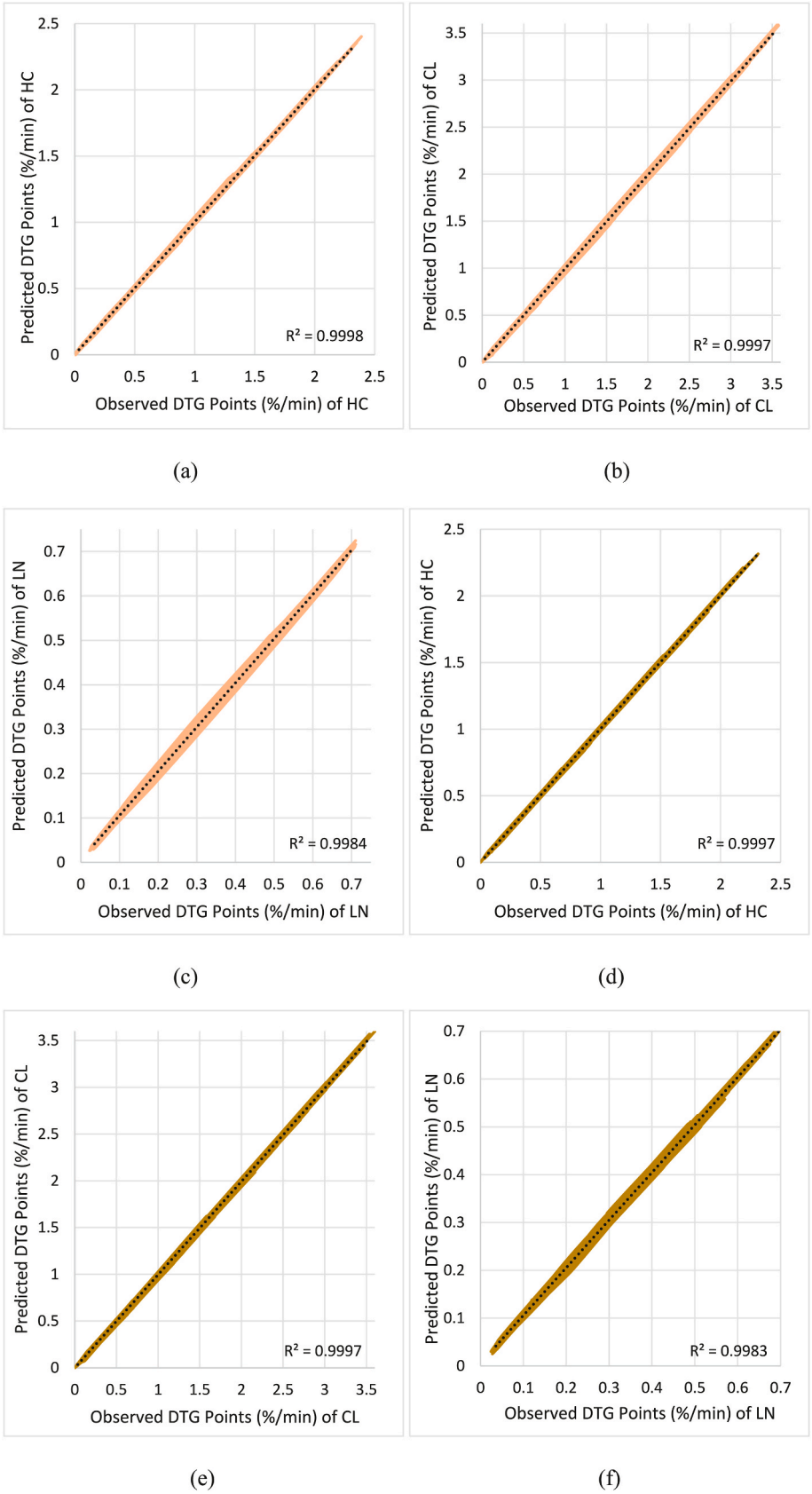

Fig. 8. R^2 scores for the training (a, b and c) and test (d, e and f).

Table 5
Results of MAPE and MSE for each target parameter in the test and training.

		HC	CL	LN
Training	**MSE**	5.444E-05	1.580E-04	6.327E-05
	MAPE	4.202	3.841	4.159
Test	**MSE**	5.248E-05	1.700E-04	6.496E-05
	MAPE	4.168	3.861	4.267

The value for mass loss in the first pyrolysis stage was almost three times higher than the value for mass loss in the second pyrolysis stage. This may be attributed to the presence of HC and CL in the feedstocks. With the exception of olive pomace, mass losses in secondary gasification were the same for all biomass samples. Olive pomace showed a mass loss of 19.82% in the secondary pyrolysis zone, about 6–7% more than the other biomass samples. This could be due to the fact that the LN content in the structure of olive pomace is higher than that in other biomass samples. In addition, the almond shell samples had a mass loss of 63.35% in the primary pyrolysis zone, resulting in a relatively high mass loss. Examination of the residual mass values showed that the approximate value was about 30%, except for almond shell and rice husk samples. This result is consistent with the biomass characteristics listed in Table 1.

Although the values calculated based on the TG curve features are more or less similar, the TG curves of the biomass samples seem to be quite different. Therefore, the amount of components degraded in these degradation regions varies. This is most evident in the DTG curves, and the DTG curve features are also shown quantitatively in Table 2. The first noticeable features are that the shoulder point of HC is at a lower temperature than the peak point of CL and that the mass loss at the CL peak (DTG_{max}) is greater. However, the parameters of these two specific points can vary greatly depending on the structure of the biomass. At the HC shoulder, the biomass with the highest mass loss per unit time is the almond shell (2.56%/min), while the biomass with the lowest mass loss is the hazelnut husk (1.11%/min). Also, the biomass with the highest DTG_{max} value is wheat straw (4.11%/min), while the lowest DTG_{max} value is hazelnut husk (2.14%/min).

3.2. Dataset

In this study, DTG data (as a function of temperature) were exported from files of thermogravimetric experiments. To exclude moisture evaporation, data before 150 °C were removed, further the data after 750 °C were not included in the calculation because no significant mass change was observed after this temperature. After visualizing the exported data, the next step is to identify the biopolymers. In most cases, three pseudo-component (HC, CL and LN) are analyzed [50], but the opposite can also be observed. For example, Meszaros et al. [51] evaluated biomass pyrolysis by considering six parallel reactions; two of them are HC and CL, and the other four macromolecules presumed to belong to lignin. Muller-Hagedorn et al. [52] considered HC and CL as two components each and LN was included as only one pseudo component while developing a model with five parallel reactions. In this paper, each biopolymer structure was assumed to have a Gaussian distribution. In fact, biopolymer degradation profiles do not exhibit symmetry around the mean, and there is always some degree of overlap between different stages of decomposition [50]. Because of this assumption, there will always be discrepancies between the

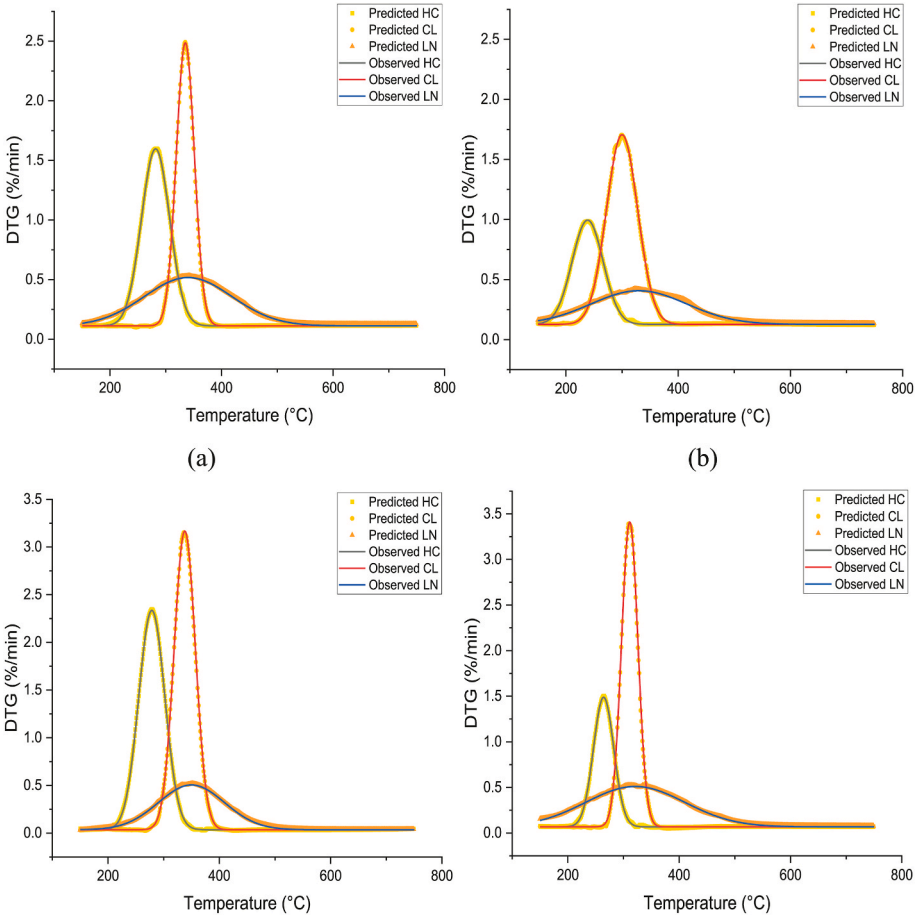

Fig. 9. Observed and estimated DTG values for the three components of each biomass sample. (a) Hazelnut Shell, (b) Hazelnut Husk, (c) Almond Shell, (d) Barley Straw, (e) Wheat Straw, (f) Olive Pomace, (g) Rice Husk, (h) Rice Straw.

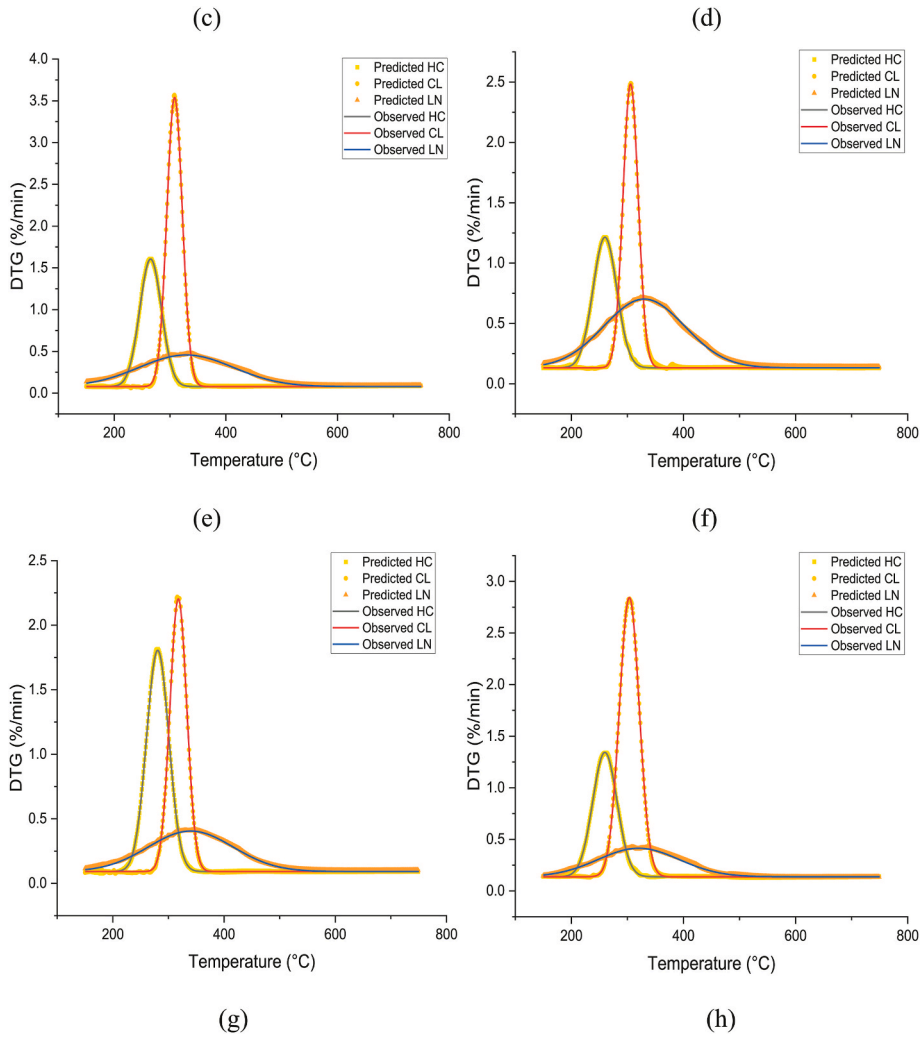

Fig. 9. (*continued*).

experimental and theoretical DTG curves that are used to fit biopolymer DTG data. Nonetheless, the Gaussian distribution is often used since it is easier to work with in a broad variety of engineering applications [53,54], and it has also been frequently used to determine the kinetic parameters of pseudo component (three biopolymers) degradation processes [55–58]. Fig. 4 illustrates the DTG curves of the experimental data and the biopolymers.

The brown "cumulative" DTG curve represents the sum of the HC, CL and LN distributions, while the black "experimental" curve represents the experimentally determined DTG data. The cumulative curve demonstrates the sum of the three biomass components with Gaussian distribution,thus, this curve is fairly smooth. The experimental curve, on the other hand, contains many noises. Therefore, there are differences between these two curves. The R^2 values for hazelnut shell, hazelnut husk, almond shell, barley straw, wheat straw, olive pomace, rice husk and rice straw samples are 0.98817, 0.98273, 0.96498, 0.99636, 0.99589, 0.98993, 0.99642 and 0.98597, respectively. The R^2 value is above 0.98 for all feedstock materials except almond shells. The results are satisfactory, although there is a deviation between the experimental and cumulative curves. After the fitting process was completed, the output values (DTG values) of the Gaussian distribution of the three biomass components were assumed to be observed values, and the training of the ANN model was performed with these values. The dataset created in this study is provided as Supplementary material.

The scientific justification for the input variables should be evident before applying statistical tools to examine the dataset. The major elements of lignocellulosic biomass are HC, CL, and LN [59], which account for approximately 90% of most lignocellulosic biomass [60]. Numerous chemical bonds in these three components are disrupted during a thermolysis process, causing the release of the VM content [15]. According to several authors [16–18], this depolymerization activity is the primary cause of VM. Furthermore, the production of aromatic compounds (particularly benzene rings) throughout thermal decomposition is crucial because it determines the production of char and the yield of char [19,20]. According to Shen et al. [21] "… *higher char yields produced from the pyrolysis of cellulose are obtained with slow heating rates*". Thus, it was concluded that the parameters of the proximate analysis of the biomass were directly connected to the biopolymers included in the composition of biomass. Numerous researchers have discovered the impacts of CL, HC, and LN on biomass VM content, ash, and FC in thermal analysis experiments. These findings make a reasonable framework for calculating the ash, VM, and FC content as ANN model input parameters. Additionally, although they have quite different characteristics, the ash, FC, and VM ratios of lignocellulosic biomass on a dry basis may be identical. The inclusion of M in the ANN model could be very useful to distinguish between biomass materials and improve the performance of the model. Furthermore, temperature is undoubtedly a key parameter, since HC, CL and LN, as mentioned earlier, have different thermal resistances (Section 3.1). This leads to different degradation behaviors of these three components at a given temperature during the thermal decomposition process. Moreover, these properties are one of the reasons why the DTG and TG curves of the

Table 6
Individual performances of biomass samples and their weight ratio in mass change.

Feedstock Material	Pseudo Component	MSE	MAPE	HC	CL	LN
Hazelnut Shell	HC	3.510E-05	3.367	34.93%	35.69%	29.61%
	CL	1.650E-04	2.348			
	LN	1.080E-04	5.772			
Hazelnut Husk	HC	5.885E-05	2.888	26.21%	48.06%	26.21%
	CL	5.627E-05	2.247			
	LN	1.160E-04	4.584			
Almond Shell	HC	6.193E-05	9.278	38.09%	42.22%	19.70%
	CL	1.680E-04	7.686			
	LN	6.096E-05	9.626			
Barley Straw	HC	5.180E-05	5.929	22.83%	43.36%	34.76%
	CL	1.630E-04	5.427			
	LN	8.514E-05	7.274			
Wheat Straw	HC	8.961E-05	8.249	27.34%	43.89%	29.26%
	CL	8.770E-05	5.521			
	LN	1.070E-04	7.162			
Olive Pomace	HC	5.106E-05	1.922	24.00%	33.34%	42.93%
	CL	1.430E-04	2.480			
	LN	9.101E-05	3.855			
Rice Husk	HC	4.497E-05	2.786	38.18%	35.42%	26.57%
	CL	5.316E-05	3.258			
	LN	6.867E-05	5.272			
Rice Straw	HC	7.116E-05	2.972	27.89%	51.04%	21.27%
	CL	1.200E-04	3.059			
	LN	7.810E-05	2.759			

biomass samples have various appearances.

Each input set in the database comprises the findings of the biomass samples' proximate analysis (wt.%, a.r.), the temperature, and the DTG points of HC, CL, and LN at the specified temperature. The DTG points for the three components range from 0.035620 to 2.335210, 0.035620–3.539750 and 0.035620–0.701270 for HC, CL and LN, respectively. Moreover, the average DTG values for HC, CL and LN in the dataset are 0.308875, 0.389425 and 0.267028, respectively. These values are also consistent with the conclusion that the mass loss per unit time is low for LN and highest for CL as explained in Section 3.1. Fig. 5 demonstrates the boxplots of the input and output parameters.

There are no outliers in the M content distribution, which ranges from 2.27% to 3.96%. Ash, on the other hand, appears to be distributed in the broadest range between the proximate analysis parameters, with a minimum of 0.85, a maximum of 19.12, and a standard deviation of 6.15. Another striking feature is that there is no possible outlier in almost any input parameter. Although outliers make it more difficult for the ANN model to forecast observed values, they assist in the testing of the model's performance for various types of biomass samples. There is a

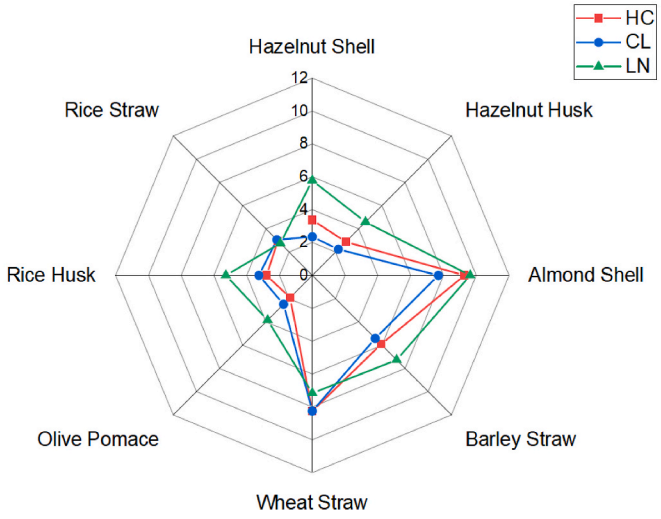

Fig. 10. Radar map of MAPE values for each biomass sample.

substantial difference in the amount of VM in other parameters of proximate analysis, which is a well-known feature of biomass [5]. There is no interesting observation regarding temperature, as the pyrolysis process was evaluated between 150 and 750 °C, as depicted in Section 3.1. The output parameters demonstrated a radically different distribution than for the input parameters. While the component LN shows no possible outliers, the components HC and CL show quite a number of possible outliers. While the decomposition of CL is in a narrow temperature range, it provides an intense peak (Fig. 4). Moreover, these peaks vary considerably depending on the biomass type. Briefly, it is understandable that there are many possible outliers within this narrow distribution. The similar behavior applies to HC since the characteristic shoulder points have been observed for different biomass samples. However, these shoulder points are not as intense as the degradation rate of CL. On the other hand, LN did not provide any possible outliers as it generally showed slow degradation over a wide temperature range. Table 3 provides a brief statistical information about the dataset created.

Examining the correlations between inputs and outputs reveals that for the modeling process, an advanced learning network needs to be developed. Although temperature and biomass characteristics certainly impact the rate of degradation of the three components, the diversity of the dataset makes it impossible to establish a linear correlation between the input and output variables. Fig. 6 illustrates the heat map for dataset created in this work.

As the temperature increased, the values of the DTG points of HC, CL and LN decreased. Since all three components have a Gaussian distribution, the decomposition rate should normally increase first and then decrease with increasing temperature. That is, it should be difficult to find a strong negative or strong positive relationship between temperature and output variables. However, a significant decrease in the rate of weight loss in the secondary pyrolysis stage and at higher temperatures led us to obtain such a result. This is also consistent with the findings that majority of the organic content of the biomass decomposes at lower temperatures and that there are significant mass losses in the primary pyrolysis zone (Section 3.1). When considering the effects of the parameters of the proximate analysis on the output variables, there is not as strong a negative or positive correlation as there is for temperature. This is because the DTG points of HC, CL and LN may have similar values for a given temperature or range of temperatures, even though the dataset contains biomass samples with different proximate analysis results. Furthermore, VM-M, VM-Ash, and FC-Ash all have a strongly negative relationship. The negative relationships between these variables may be explained simply by the mathematical fact that on an as received basis, the total of the proximate analysis results should be equal

to one hundred. The positive correlation between the DTG points of CL and LN may be due to the relative closeness of the peak values of these two components and the relatively similar rise/fall. On the other hand, the situation between HC and CL is reversed, since in the temperature ranges where the rate of degradation of CL begins to increase, the rate of degradation of HC begins to decrease. Additionally, a positive correlation can be mentioned between HC and LN, but it is not as strong as the positive correlation between CL and LN. In conclusion, establishing a linear connection is difficult owing to the complex relationships between inputs and outputs. However, even if there is no direct correlation between input and output data, this does not mean that there is no other kind of interaction. An advanced learning system, such as ANN, can be put up to solve this problem.

3.3. Assessment of the ANN model

Using the open-source library "TensorFlow" [61], the DTG points of LN, CL, and HC were evaluated using an ANN model developed in Python software. The created dataset (8000 datasets) was divided into subsets to improve the generalization performance: 80% for the training (6400 datasets) and 20% for the test (1600 datasets). Because there is no precise way for determining the number of neurons in hidden layers, the trial-and-error technique was preferred. The topology of the ANN consists of an input layer (5 neurons), two hidden layers (150 and 100 neurons) and an output layer (3 neurons), as visualized in Fig. 7.

Temperature, M, FC, VM, and Ash are the five parameters in the input layer. The first hidden layer has 150 neurons, whereas the second hidden layer contains 100 neurons that receive input data from the first hidden layer. Each neuron adds a bias number to the output after multiplying a weight value by the input set it receives. The input data were transmitted into the model in batches of 10 in this research. In the first hidden layer, the activation function ReLU was preferred and in the second hidden layer, the activation function SELU was preferred. The DTG points (%/min) of HC, CL, and LN were derived from the data source in the hidden layers and proceed to the output layer. Using an optimizer, the model's parameters were changed with iterations. Based on the result of the loss function, an optimizer determines how to adjust the network weights. Table 4 summarizes the ANN's parameters.

To obtain the best results for the training and testing datasets, the parameters of the ANN model hyperparameters were optimized to minimize MSE. A random selection of data was utilized to train the ANN model, and then a test phase was conducted to evaluate the effectiveness of the network with a different dataset than the one used in training. To achieve acceptable predictive accuracy, the process was repeated until the MSE value fell below a predetermined threshold. The R^2 indicates the relationship between the predicted and observed results. A comparison of the DTG points of HC, CL, and LN is shown in Fig. 8.

The training and test datasets were randomly determined during the training section of the neural network. The results related to the predictive ability of the neural network showed that the model was properly fitted for training and testing, as the R^2 values were above 0.998. The high R^2 values show that the observed DTG points of HC, CL, and LN have a good agreement with the predicted values. The test R^2 values are slightly lower than the training R^2 values, but the predictive ability of the model is still quite satisfactory. The satisfactory test and training results indicate that the developed ANN model is an influential model for estimating the DTG points of three components for different biomass types and at a specific temperature. The effectiveness of the ANN model can be further understood by examining the MSE and MAPE values, which are also considered as performance metrics in addition to R^2. Table 5 shows the MAPE and MSE values from testing and training.

The reliable performance of ANN in both training and testing for all three components suggests that there is no overfitting. In addition, the component with the most successful prediction of DTG points during thermolysis appears to be CL, whereas the component with the highest MAPE value during testing is LN. The DTG points can be easily predicted because CL decomposes rapidly in a narrow temperature range. On the other hand, LN has a slow decomposition characteristic throughout the pyrolysis, but may vary depending on the biomass characteristics. This could be the reason why the highest MAPE and the lowest R^2 values were obtained for LN. However, all MSE values for all three components are relatively low and MAPE values are less than 4.5%. Fig. 9 is also included to evaluate the performance of the neural network model for each biomass sample.

The solid line shows the observed DTG points, whereas the dots represent the predicted DTG points. While ANN performs well in both training and testing the randomly split overall dataset, the performance for each individual biomass sample is also satisfactory. This also shows that the neural network can simulate the HC, CL and LN degradation trend considering the biomass properties. Furthermore, by summing the integral areas of the Gaussian distribution of these three components, the integral area of the cumulative curve (Section 3.2) can be calculated. In this way, the contributions of HC, CL, and LN to the mass change occurring during pyrolysis can also be calculated. Table 6 shows the mass values (%) for the three components and the values of the statistical performance indicators.

When evaluating the individual performance of each biomass, we note that the MAPE values of HC, CL, and LN are below 10%. The biomasses with the highest MAPE values seem to be almond shell, barley straw and wheat straw. In fact, the proximate analysis results of these three biomasses are not outliers, only the ash content of almond shell is relatively low. However, biomass with similar ash content is also included in the dataset. Features of the DTG curves could be the reason for the relatively high error. The HC distribution of almond shell covers most of the cumulative area. Moreover, the distribution of LN starts slightly at a higher temperature. This causes it to have a different DTG behavior than other biomass samples. Fig. 10 shows the MAPE values of the biomass samples on the radar map.

As can be seen in Fig. 10, the almond shell, barley straw, and wheat straw are relatively far from the center. It is also noticeable that the MAPE values of the LN of the hazelnut shell and rice husk samples are relatively higher than the MAPE values of the HC and CL samples. As a general behavior, it can be mentioned that the MAPE values are ordered from the largest to the smallest value: LN > HC > CL. This ranking suggests that while the ANN model can estimate the behavior of components that lose mass rapidly over a narrow temperature range, it is relatively weak in predicting the behavior of components that degrade slowly over a wide temperature range. In addition, although there are characteristic images of HC and CL, such as shoulders and peaks, there is no indicator for LN, and the thermal degradation of LN can only be determined by estimation. Nevertheless, the performance of the ANN model in simulating the thermogravimetric behavior of the three major components is quite impressive.

When the values for the weight percentages of HC, CL, and LN are examined, it is found that the values of these three components are consistent with those reported in the literature [62]. The percentages by weight of HC are within a reasonable range, with the exception of almond shell (38.09%) and rice husk (38.18%). Nevertheless, these values are not extreme. Moreover, the mass values of the component CL are the most compatible within the range reported in the literature. Only the rice straw (51.04%) is outside this range by almost 1%. Finally, LN stands out as the component that is most above the indicated range (25%). In fact, the LN weight percentages of the biomass samples are acceptable, except for barley straw (34.76%) and olive pomace (42.93%). The area of LN had to increase to achieve a good fit, and thus the area under the curve increased dramatically. It can be concluded that the massive mass fraction resulting from the relatively high weight loss in the secondary pyrolysis stage may be the reason for estimating such high amounts of LN, especially for the olive pomace sample.

4. Conclusion

Understanding the thermal degradation of biopolymers in biomass is important to optimize the conversion of biomass into useful products and to develop innovative renewable energy technologies. In this study, a novel model based on ANN was developed to estimate the curves of thermal degradation of biopolymers in biomass. Although models have already been developed for predicting HC, CL, and LN, there is no study that directly simulates the degradation behavior of these three biopolymers at a specific temperature or temperature range. Furthermore, the area under the curves formed by the neural network calculations can be used to predict how much degradation will occur for which biopolymers. The performance of the model is quite satisfactory in simulating the degradation curves of biomass components, with R^2 values above 0.998 in both training and testing. The results provide an alternative perspective for understanding the thermal degradation of biopolymers in biomass, which may contribute to the development of new renewable energy technologies and processes for lignocellulosic fuels.

CRediT authorship contribution statement

Furkan Kartal: Data curation, Investigation, Software, Validation, Visualization, Writing. **Yağmur Dalbudak:** Validation, WritingWriting. **Uğur Özveren:** Conceptualization, Data curation, Investigation, Methodology, Project administration, Resources, Software, Supervision, Validation, Visualization, WritingWriting.

Declaration of competing interest

The authors declare that they have no known competing financial interests or personal relationships that could have appeared to influence the work reported in this paper.

Appendix A. Supplementary data

Supplementary data to this article can be found online at https://doi.org/10.1016/j.renene.2023.01.017.

References

[1] M. Asif, T. Muneer, Energy supply, its demand and security issues for developed and emerging economies, Renew. Sustain. Energy Rev. 11 (7) (2007) 1388–1413.
[2] C.a. Wang, X. Zhang, Y. Liu, D. Che, Pyrolysis and combustion characteristics of coals in oxyfuel combustion, Appl. Energy 97 (2012) 264–273.
[3] S. Wang, G. Dai, H. Yang, Z. Luo, Lignocellulosic biomass pyrolysis mechanism: a state-of-the-art review, Prog. Energy Combust. Sci. 62 (2017) 33–86.
[4] A. Sarvaramini, G.P. Assima, G. Beaudoin, F. Larachi, Biomass torrefaction and CO2 capture using mining wastes–A new approach for reducing greenhouse gas emissions of co-firing plants, Fuel 115 (2014) 749–757.
[5] C. Sheng, J. Azevedo, Modeling biomass devolatilization using the chemical percolation devolatilization model for the main components, Proc. Combust. Inst. 29 (1) (2002) 407–414.
[6] P. Nimmanterdwong, B. Chalermsinsuwan, P. Piumsomboon, Prediction of lignocellulosic biomass structural components from ultimate/proximate analysis, Energy 222 (2021), 119945.
[7] B.C. Saha, Hemicellulose bioconversion, J. Ind. Microbiol. Biotechnol. 30 (5) (2003) 279–291.
[8] F. Hu, A. Ragauskas, Pretreatment and lignocellulosic chemistry, Bioenergy Research 5 (4) (2012) 1043–1066.
[9] C. Sawatdeenarunat, K. Surendra, D. Takara, H. Oechsner, S.K. Khanal, Anaerobic digestion of lignocellulosic biomass: challenges and opportunities, Bioresour. Technol. 178 (2015) 178–186.
[10] A. Toscan, A.R.C. Morais, S.M. Paixao, L. Alves, J. Andreaus, M. Camassola, A.J. P. Dillon, R.M. Lukasik, High-pressure carbon dioxide/water pre-treatment of sugarcane bagasse and elephant grass: assessment of the effect of biomass composition on process efficiency, Bioresour. Technol. 224 (2017) 639–647.
[11] H. Goyal, D. Seal, R. Saxena, Bio-fuels from thermochemical conversion of renewable resources: a review, Renew. Sustain. Energy Rev. 12 (2) (2008) 504–517.
[12] M. Van de Velden, J. Baeyens, A. Brems, B. Janssens, R. Dewil, Fundamentals, kinetics and endothermicity of the biomass pyrolysis reaction, Renew. Energy 35 (1) (2010) 232–242.
[13] F. Shafizadeh, Introduction to pyrolysis of biomass, J. Anal. Appl. Pyrol. 3 (4) (1982) 283–305.
[14] A. Demirbaş, Mechanisms of liquefaction and pyrolysis reactions of biomass, Energy Convers. Manag. 41 (6) (2000) 633–646.
[15] F.-X. Collard, J. Blin, A review on pyrolysis of biomass constituents: mechanisms and composition of the products obtained from the conversion of cellulose, hemicelluloses and lignin, Renew. Sustain. Energy Reviews 38 (2014) 594–608.
[16] A.M. Azeez, D. Meier, J. Odermatt, Temperature dependence of fast pyrolysis volatile products from European and African biomasses, J. Anal. Appl. Pyrol. 90 (2) (2011) 81–92.
[17] J. Lédé, F. Blanchard, O. Boutin, Radiant flash pyrolysis of cellulose pellets: products and mechanisms involved in transient and steady state conditions, Fuel 81 (10) (2002) 1269–1279.
[18] V. Mamleev, S. Bourbigot, M. Le Bras, J. Yvon, The facts and hypotheses relating to the phenomenological model of cellulose pyrolysis: interdependence of the steps, J. Anal. Appl. Pyrol. 84 (1) (2009) 1–17.
[19] T.E. McGrath, W.G. Chan, M.R. Hajaligol, Low temperature mechanism for the formation of polycyclic aromatic hydrocarbons from the pyrolysis of cellulose, J. Anal. Appl. Pyrol. 66 (1–2) (2003) 51–70.
[20] I. Pastorova, R.E. Botto, P.W. Arisz, J.J. Boon, Cellulose char structure: a combined analytical Py-GC-MS, FTIR, and NMR study, Carbohydr. Res. 262 (1) (1994) 27–47.
[21] D. Shen, S. Gu, The mechanism for thermal decomposition of cellulose and its main products, Bioresour. Technol. 100 (24) (2009) 6496–6504.
[22] X. Jin, X. Chen, C. Shi, M. Li, Y. Guan, C.Y. Yu, T. Yamada, E.J. Sacks, J. Peng, Determination of hemicellulose, cellulose and lignin content using visible and near infrared spectroscopy in Miscanthus sinensis, Bioresour. Technol. 241 (2017) 603–609.
[23] L. Peng, C.H. Hocart, J.W. Redmond, R.E. Williamson, Fractionation of carbohydrates in Arabidopsis root cell walls shows that three radial swelling loci are specifically involved in cellulose production, Planta 211 (3) (2000) 406–414.
[24] N. Xu, W. Zhang, S. Ren, F. Liu, C. Zhao, H. Liao, Z. Xu, J. Huang, Q. Li, Y. Tu, Hemicelluloses negatively affect lignocellulose crystallinity for high biomass digestibility under NaOH and H2SO4 pretreatments in Miscanthus, Biotechnol. Biofuels 5 (1) (2012) 1–12.
[25] M. Schwanninger, J.C. Rodrigues, N. Gierlinger, B. Hinterstoisser, Determination of lignin content in Norway spruce wood by Fourier transformed near infrared spectroscopy and partial least squares regression. Part 1: wavenumber selection and evaluation of the selected range, J. Near Infrared Spectrosc. 19 (5) (2011) 319–329.
[26] X. Li, C. Sun, B. Zhou, Y. He, Determination of hemicellulose, cellulose and lignin in moso bamboo by near infrared spectroscopy, Sci. Rep. 5 (1) (2015) 1–11.
[27] H. Sharma, Compositional analysis of neutral detergent, acid detergent, lignin and humus fractions of mushroom compost, Thermochim. Acta 285 (2) (1996) 211–220.
[28] J.B. Sluiter, R.O. Ruiz, C.J. Scarlata, A.D. Sluiter, D.W. Templeton, Compositional analysis of lignocellulosic feedstocks. 1. Review and description of methods, J. Agric. Food Chem. 58 (16) (2010) 9043–9053.
[29] L. Wu, M. Li, J. Huang, H. Zhang, W. Zou, S. Hu, Y. Li, C. Fan, R. Zhang, H. Jing, A near infrared spectroscopic assay for stalk soluble sugars, bagasse enzymatic saccharification and wall polymers in sweet sorghum, Bioresour. Technol. 177 (2015) 118–124.
[30] L. Liu, X.P. Ye, A.R. Womac, S. Sokhansanj, Variability of biomass chemical composition and rapid analysis using FT-NIR techniques, Carbohydr. Polym. 81 (4) (2010) 820–829.
[31] J. Xing, K. Luo, H. Wang, J. Fan, Estimating biomass major chemical constituents from ultimate analysis using a random forest model, Bioresour. Technol. 288 (2019), 121541.
[32] A.G. Barneto, J.A. Carmona, J.A. Conesa, Effects of the composting and the heating rate on biomass gasification, Energy Fuel. 23 (2) (2009) 951–957.
[33] Z. Yang, K. Li, M. Zhang, D. Xin, J. Zhang, Rapid determination of chemical composition and classification of bamboo fractions using visible–near infrared spectroscopy coupled with multivariate data analysis, Biotechnol. Biofuels 9 (1) (2016) 35.
[34] M. Carrier, A. Loppinet-Serani, D. Denux, J.-M. Lasnier, F. Ham-Pichavant, F. Cansell, C. Aymonier, Thermogravimetric analysis as a new method to determine the lignocellulosic composition of biomass, Biomass Bioenergy 35 (1) (2011) 298–307.
[35] M. Radojević, B. Janković, V. Jovanović, D. Stojiljković, N. Manić, Comparative pyrolysis kinetics of various biomasses based on model-free and DAEM approaches improved with numerical optimization procedure, PLoS One 13 (10) (2018), e0206657.
[36] L. Lu, S. Devasahayam, V. Sahajwalla, Evaluation of Coal for Metallurgical Applications, the Coal Handbook: towards Cleaner Production, 2013, pp. 352–386.
[37] S.K. Jain, V.P. Singh, Water Resources Systems Planning and Management, Elsevier, 2003.
[38] M. Aghbashlo, W. Peng, M. Tabatabaei, S.A. Kalogirou, S. Soltanian, H. Hosseinzadeh-Bandbafha, O. Mahian, S.S. Lam, Machine learning technology in biodiesel research: a review, Prog. Energy Combust. Sci. 85 (2021), 100904.
[39] A. Dongare, R. Kharde, A.D. Kachare, Introduction to artificial neural network, Int. J. Eng. Innovative Technol.(IJEIT) 2 (1) (2012) 189–194.
[40] K. Atsonios, A. Nesiadis, N. Detsios, K. Koutita, N. Nikolopoulos, P. Grammelis, Review on dynamic process modeling of gasification based biorefineries and bio-based heat & power plants, Fuel Process. Technol. 197 (2020), 106188.
[41] A. Shrestha, A. Mahmood, Review of deep learning algorithms and architectures, IEEE Access 7 (2019) 53040–53065.
[42] A. Krizhevsky, I. Sutskever, G.E. Hinton, Imagenet classification with deep convolutional neural networks, CA 60 (6) (2017) 84–90.

[43] G. Klambauer, T. Unterthiner, A. Mayr, S. Hochreiter, Self-normalizing neural networks, Adv. Neural Inf. Process. Syst. 30 (2017).
[44] D.P. Kingma, J. Ba, Adam: A Method for Stochastic Optimization, 2014 arXiv preprint arXiv:1412.6980.
[45] T. Chauhan, H. Palivela, S. Tiwari, Optimization and fine-tuning of DenseNet model for classification of covid-19 cases in medical imaging, Int. J. Information Manag. Data Insights 1 (2) (2021), 100020.
[46] A. Kanca, Investigation on pyrolysis and combustion characteristics of low quality lignite, cotton waste, and their blends by TGA-FTIR, Fuel 263 (2020), 116517.
[47] L. TranVan, V. Legrand, F. Jacquemin, Thermal decomposition kinetics of balsa wood: kinetics and degradation mechanisms comparison between dry and moisturized materials, Polym. Degrad. Stabil. 110 (2014) 208–215.
[48] C. Zhang, S. Li, S. Ouyang, C.-W. Tsang, D. Xiong, K. Yang, Y. Zhou, Y. Xiao, Co-pyrolysis characteristics of camellia oleifera shell and coal in a TGA and a fixed-bed reactor, J. Anal. Appl. Pyrol. (2021), 105035.
[49] M. Mureddu, F. Dessì, A. Orsini, F. Ferrara, A. Pettinau, Air-and oxygen-blown characterization of coal and biomass by thermogravimetric analysis, Fuel 212 (2018) 626–637.
[50] C. Di Blasi, Modeling chemical and physical processes of wood and biomass pyrolysis, Prog. Energy Combust. Sci. 34 (1) (2008) 47–90.
[51] S. Alves, J. Figueiredo, Pyrolysis kinetics of lignocellulosic materials by multistage isothermal thermogravimetry, J. Anal. Appl. Pyrol. 13 (1–2) (1988) 123–134.
[52] M. Müller-Hagedorn, H. Bockhorn, L. Krebs, U. Müller, A comparative kinetic study on the pyrolysis of three different wood species, J. Anal. Appl. Pyrol. 68 (2003) 231–249.
[53] A. Dasgupta, A. Wahed, Laboratory Statistics and Quality Control, Clinical Chemistry, Immunology and Laboratory Quality Control, Elsevier, 2014, p. 10.
[54] T.B. Farver, Concepts of Normality in Clinical Biochemistry, Clinical biochemistry of domestic animals, 1997, pp. 1–19. Elsevier.
[55] J. Kristanto, M.M. Azis, S. Purwono, Multi-distribution activation energy model on slow pyrolysis of cellulose and lignin in TGA/DSC, Heliyon 7 (7) (2021), e07669.
[56] J.J. Orfão, F.J. Antunes, J.L. Figueiredo, Pyrolysis kinetics of lignocellulosic materials—three independent reactions model, Fuel 78 (3) (1999) 349–358.
[57] T. Menares, J. Herrera, R. Romero, P. Osorio, L.E. Arteaga-Pérez, Waste tires pyrolysis kinetics and reaction mechanisms explained by TGA and Py-GC/MS under kinetically-controlled regime, Waste Manag. 102 (2020) 21–29.
[58] R. Huang, Z. Teng, S. Li, Gaussian model analysis and thermal decomposition kinetics of nature fibers, J. Clean. Prod. 357 (2022), 131784.
[59] S. Chen, Y. Xia, B. Zhang, H. Chen, G. Chen, S. Tang, Disassembly of lignocellulose into cellulose, hemicellulose, and lignin for preparation of porous carbon materials with enhanced performances, J. Hazard Mater. 408 (2021), 124956.
[60] W.-H. Chen, C.F. Eng, Y.-Y. Lin, Q.-V. Bach, V. Ashokkumar, P.-L. Show, Two-step thermodegradation kinetics of cellulose, hemicelluloses, and lignin under isothermal torrefaction analyzed by particle swarm optimization, Energy Convers. Manag. 238 (2021), 114116.
[61] M. Abadi, P. Barham, J. Chen, Z. Chen, A. Davis, J. Dean, M. Devin, S. Ghemawat, G. Irving, M. Isard, Tensorflow: A System for Large-Scale Machine Learning, 12th {USENIX} Symposium on Operating Systems Design and Implementation, 2016, pp. 265–283 ({OSDI} 16).
[62] L. Reyes, L. Abdelouahed, C. Mohabeer, J.-C. Buvat, B. Taouk, Energetic and exergetic study of the pyrolysis of lignocellulosic biomasses, cellulose, hemicellulose and lignin, Energy Convers. Manag. 244 (2021), 114459.